Journal of Structural Biology 184 (2013) 164–172

Contents lists available at ScienceDirect

Journal of Structural Biology

journal homepage: www.elsevier.com/locate/yjsbi

Bone quality around bioactive silica-based coated stainless steel implants: Analysis by Micro-Raman, XRF and XAS techniques

Josefina Ballarre [a,*], Paula M. Desimone [a], Matthieu Chorro [b], Matías Baca [c], Juan Carlos Orellano [c], Silvia M. Ceré [a]

[a] INTEMA, Universidad Nacional del Mar del Plata-CONICET, Juan B. Justo 4302, B7608FDQ Mar del Plata, Argentina
[b] LUCIA Beamline – Synchrotron SOLEIL, Saint Aubin, France
[c] Traumatología y Ortopedia, Hospital Interzonal General de Agudos "Oscar Alende", Mar del Plata, Argentina

ARTICLE INFO

Article history:
Received 22 July 2013
Received in revised form 12 September 2013
Accepted 13 September 2013
Available online 27 September 2013

Keywords:
Coatings
Surgical grade stainless steel
Newly-formed bone
Raman
Synchrotron radiation

ABSTRACT

Surface modification of surgical stainless steel implants by sol gel coatings has been proposed as a tool to generate a surface that besides being protective could also create a "bioactive" interface to generate a natural bonding between the metal surface and the existing bone. The aim of this work is to analyze the quality and bone formation around hybrid bioactive coatings containing glass-ceramic particles, made by sol–gel process on 316L stainless steel used as permanent implant in terms of mineralization, calcium content and bone maturity with micro Raman, X-ray microfluorescence and X-ray absorption techniques. Uncoated implants seem to generate a thin bone layer at the beginning of osseointegration process and then this layer being separated from the surface with time. The hybrid coatings without glass-ceramic particles generate new bone around implants, with high concentration of Ca and P at the implant/tissue interface. This fact seems to be related with the presence of silica nanoparticles in the layer. The addition of bioactive particles promotes and enhances the bone quality with a homogeneous Ca and P content and a low rate of beta carbonate substitution and crystallinity, similar to young and mechanical resistant bone.

1. Introduction

Orthopaedic devices for permanent implants required short term fixation and fast bone attachment and healing. Also they are required to have excellent mechanical properties in load bearing sites and to be corrosion resistant. Metallic alloys used in surgery share, in common, high mechanical resistance (Hastings, 1980) and high corrosion resistance in physiologic media mainly due to the formation of a passive oxide film that reduces the corrosion rate by blocking the transport and the possible migration of metallic ions from the base metal to the nearby tissue (Hanawa, 2004). Surface modification of surgical implants by sol gel coatings has been proposed as a tool to generate a surface that besides being protective could also allow the integration of the metal to the human body, generating a "bioactive" interface that has the ability of create a natural bonding between the metal surface and the existing bone. It has been demonstrated that inorganic – hybrid SiO_2 coatings, obtained from tetraethylorthosilicate (TEOS) and methyltriethoxysilane (MTES) improve the corrosion behaviour of the AISI 316L stainless steel in biological environments (Ballarre et al., 2007; Checmanowski and Szczygiel, 2008; Chou et al., 2003). The hybrid layers of TEOS and other silanes are not bioactive per se but if the coatings are also functionalized with a bioactive ceramic or glass-ceramic from the $CaO–SiO_2–P_2O_5$ system, it has been proved that the HA rate can be maximized (Höland, 1997; Kokubo et al., 1992; Peitl et al., 2001). Silica is also known as a natural catalyst for hydroxyapatite formation (HA: $Ca_{10}(PO_4)_6(OH)_2$), showing bioactivity *in vitro* (Beck et al., 2012; Hing et al., 2006).

Bone is a composite material consisting of an organic component of the matrix mainly type I collagen assembled fibrils, impregnated and surrounded by small nano-particles of HA (Fratzl et al., 2004). It is well established that bone mineral resembles a poorly crystalline form of the HA, with contain other ions, especially carbonates (Harries et al., 1988). The analysis of *in vivo* formation of new tissue at the interfaces of bioactive implants has been reported using histological methods. Also the interfacial mechanical properties, such as stiffness have been studied (Coathup et al., 2001). Contributions of the mineral phase to the mechanics of bone are investigated in great detail in terms of, for example, the degree of mineralization. It has been demonstrated that mineralization affects bone tissue mechanics, and therefore it is necessary to use different techniques focused at the micro-nano structural and

* Corresponding author. Address: INTEMA, Corrosion Division, UNMdP, Juan B. Justo 4302, B7608FDQ, Mar del Plata, Argentina. Fax: +54 223 4810046.
E-mail address: jballarre@fi.mdp.edu.ar (J. Ballarre).

1047-8477/$ - see front matter © 2013 Elsevier Inc. All rights reserved.
http://dx.doi.org/10.1016/j.jsb.2013.09.016

chemical level to determine degrees of tissue mineralization (Currey, 2004). The use of soft (0.8–8 keV) X-ray microprobe (with synchrotron radiation) with capabilities of chemical speciation by micro-X-ray absorption spectroscopy (μ-XAS) and elemental mapping by X-ray microfluorescence (μ-XRF) allows to study heterogeneous samples at the micrometer scale in a non-destructive way (Flank et al., 2006).

The aim of this work is to analyze the fixation and bone formation around bioactive coatings made by sol–gel technique on 316L stainless steel used as permanent implant in terms of mineralization, calcium content and bone maturity with micro Raman, X-ray microfluorescence and X-ray absorption techniques. The effect of having hybrid organic-inorganic protective silica based layer with or without bioactive particles in terms of bone formation is investigated.

2. Materials and methods

2.1. Materials

Stainless steel AISI 316L (Atlantic Stainless Co. Inc., Massachusetts, US) in form of cylinders of 1.3 mm diameter and 2 cm length were used as substrates. The composition of the steel was: C 0.03% max, Mn 2% max, Si 1% max, P 0.045% max, S 0.03% max, Ni 10–14%, Cr 16–18%, Mo 2–3%, balance Fe. Samples were degreased, washed with distilled water, and rinsed in ethanol before coating.

2.1.1. Preparation of the coating sols

Hybrid organic–inorganic sols were prepared with a silicon tetraethylorthosilane (TEOS, 99%, ABCR GmbH & Co, Germany), methyltriethoxysilane (MTES, 98%, ABCR GmbH & Co, Germany) and a water based solution with colloidal silica (LEVASIL 200A 40 wt.%, Bayer, Germany), called from now on SiO_2:col. The molar ratio of the silanes were maintained constant (TEOS/MTES = 40/60), the concentration of colloidal silica was 10 mol% with respect to the total amount of silica and nitric acid (0.1 mol.L^{-1}) was used as catalyser. The final silica concentration for both sols was 4.16 mol.L^{-1}.

2.1.2. Glass-ceramic (GC) particles and suspension

The glass-ceramic particles were made from a precursor glass system SiO_2–P_2O_5–CaO. Silica sand, calcium carbonate (Aldrich) and orthophosphoric acid (Aldrich) were used as precursors. The ratio of components was calculated in order to obtain the weight concentration of CaO 47.29%, SiO_2 35.69% and P_2O_5 17.01% in the final glass. The mixture was fused in a platinum crucible at 1600 °C in air atmosphere, and then quenched in water. The thermal treatment of glass was made at 1050 °C for 2 h in an electric furnace with the aim of obtaining apatite and wollastonite as crystalline phases. The GC obtained was milled in an agate planetary mill (Fritsch Pulverisette, Germany), at a rotation speed of 1500 rpm for 4 h and the powder was sieved with Tyler screens (grades 270, 325 and 600) to obtain a diameter size distribution of less than 20 μm. The particle suspensions were prepared by the adding 10 wt.% of GC particles to the TEOS-MTES-SiO_2:col sol. The suspensions were stirred by a high shear mixing in a rotor-stator agitator (Silverson L2R, UK) for 6 min and 15 wt.% of solids of a surfactant was added.

2.1.3. Coating

All the samples were prepared as a double layer system. A first layer prepared with TEOS-MTES-SiO_2:col sol was obtained at room temperature by dip-coating at a withdrawal rate of 25 cm min^{-1}, dried at room temperature for 30 min, and heat treated for 30 min at 450 °C in an electric furnace. A second layer was made applying TEOS-MTES-SiO_2:col with or without 10 wt.% GC particles on the top of the first one (called TMS and TMS-GC, respectively). The withdrawal and thermal treatment conditions used was the same as in the first layer. A scheme of coating deposition is shown in Fig. 1, and the names of the samples used are detailed in Table 1.

2.2. In vivo experiments and analysis

2.2.1. Implantation

In vivo experiments were conducted in total in 6 Wistar – Hokkaido (WKAH/Hok) adult rats (weight 350 ± 50 g), according to rules of ethical committee of the National University of Mar del Plata (Interdisciplinary Committee, April 2005/October 2010), taking care of surgical procedures, pain control, standards of living and appropriately human methods of sacrifice of test animals. Coated and uncoated wires were sterilized in autoclave for 20 min at 121 °C. Rats were anaesthetized with fentanyl citrate and droperidol (Janssen-Cilag Lab, Johnson and Johnson, Madrid, Spain) according to their weight and the region of surgery surface was cleaned with antiseptic soap. The animals were placed in a supine position and the implantation site was exposed. A region of around 0.5 cm diameter was scraped in the femur plateau and a hole was drilled using a hand drill of 0.125 cm diameter bur at low speed. The implantation site was irrigated with physiological saline solution during the drilling procedure for cleaning and

Table 1
Type of implants (coated samples) analyzed.

Sample name	First layer	Second layer
SS	–	–
TMS	TEOS-MTES-SiO_2:col	TEOS-MTES-SiO_2:col
TMS-GC	TEOS-MTES-SiO_2:col	TEOS-MTES-SiO_2:col + glass-ceramic particles (GC)

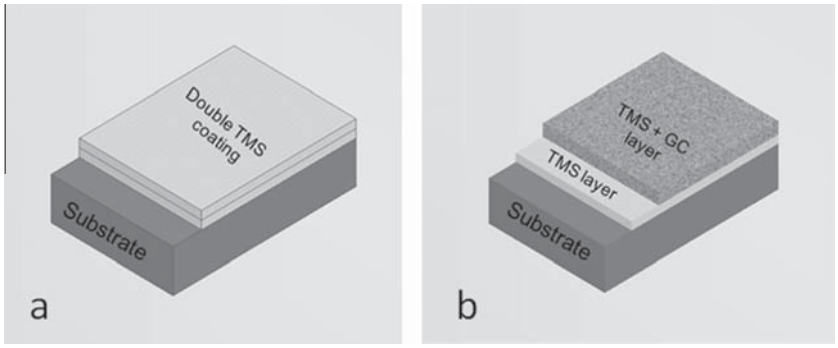

Fig.1. Graphic scheme of the hybrid coating system on AISI 316 stainless steel substrates: (a) TMS double coating, (B) TMS-GC double layer system.

cooling proposes. The coated implants and uncoated wire implants, as controls, were placed by press fit into femur extending into the medullar canal. The animals were sacrificed with an overdose of intraperitoneal fentanyl citrate and droperidol after 60 days and the bone with implants were retrieved. Conventional X-ray radiographs were taken before retrieving the samples for control purposes.

2.2.2. Samples sectioning

The retrieved samples were cleaned from surrounding soft tissues and fixed in neutral 10 wt.% formaldehyde for 24 h. Then they were dehydrated in a series of alcohols (70%, 85%, 95% and 100%) followed by a methacrylated solution and finally embedded in poly-methyl methacrylate (PMMA) solution and polymerized for 7 days at 32 °C. The PMMA embedded blocks were cut with a low speed diamond blade saw (Buehler GmbH) cooled with water. Various sections were made according to the different analysis requirements, with thickness varying from 80 to 250 μm.

2.2.3. Histological analysis

To observe the soft tissue and the bone lining cells, the histological sections were stained with 20% Giemsa stain solution. The stained samples sections were observed by optical light microscope (Leica DM RXA2).

2.2.4. XRF and EXAFS measurements

XAS experiments were carried out at LUCIA beamline, Synchrotron Soleil, France (Flank et al., 2006). X-ray energy was selected with a double Si (1 1 1) monochromator and X-ray beam was focused with KB mirrors apparatus down to $3 \times 5\ \mu m^2$. Fluorescence measurements were performed with a four elements silicon drift detector (Xflash detector 5040, Bruker company). Elementary Fluorescence Maps (following the intensity of the Kα line of Fe, Cr, Ca, P and Si) were performed with steps of 3 μm in vertical and horizontal directions. Two excitation energies were used: 7200 eV (above Fe K edge) or 4100 eV (above Ca K edge) in order to be sensitive to the implant elements Fe, Cr or to the bone elements Ca, P and Si. After mapping, EXAFS spectra were collected at Ca K edge (4038 eV) and fluorescence mode on points of interest defined in the marrow and the cortical zone of the bone. All measurements were done in reflection mode, under vacuum and at room temperature. For data evaluation, the ATHENA program was used, which is included in the IFEFFIT package for XAS analysis.

2.2.5. Micro-Raman analysis

Two slices of the same section of each animal were analyzed by Raman using a inVia spectrometer (Renishaw, UK) system equipped with charge-coupled device (CCD) detector of 1040×256 pixels and coupled to a Leica microscope (DM-2500 model) (50x, 0.75 NA) with a computer-controlled *x–y–z* stage. A diode laser line (785 nm) was used as excitation source in combination with a grating of 1200 grooves/mm. The laser power was kept below 10% to avoid sample damage, employing one 30-sec acquisition for each data point. The spectral resolution was $4\ cm^{-1}$, and the spectra were taken from 300 to $1800\ cm^{-1}$. For each bone sample, two sets of spectra were collected: one near the implant in the newly formed bone zone, where the implant was only in contact to the marrow, and other in the existing cortical bone. Each set was comprised of a 4×5 grid of spectra that were averaged and statistically analyzed.

For better understanding of the chemical and compositional changes at the interface, line scans were collected starting from the metallic implant, passing through the newly formed bone and finishing in the marrow. The total length of the spectra was 200 μm, taking a spectrum every 10 μm. The measurement conditions were the same as for the previous scans (785 nm laser, 300–1800 cm^{-1} scan, resolution 4 cm^{-1}, 30 s acquisition time).

Background fluorescence in the spectra was subtracted by a modified polynomial fitting algorithm. Peak intensities were recorded for amide I (1650 cm^{-1}), amide III (1245 cm^{-1}), B-type carbonate (1071 cm^{-1}), ν1 phosphate (960 cm^{-1}), and ν2 phosphate (430 cm^{-1}) using a custom developed Matlab program. The mineral to matrix ratio was calculated based on the intensity ratio of the ν1 phosphate peak to either the amide I or CH2 wag, and the ν2 phosphate peak to amide III peak intensity. Carbonate concentration in calcified tissues varies with the type of tissue (enamel, dentine, bone), maturity, crystallinity, and the bone structural features such as age and history of fracture. Vibrational spectroscopies (infrared and Raman) are ideal methods for analyzing mineral structure because they are sensitive to changes in crystallinity and molecular substitution. The ratio of the carbonate peak to the ν2 phosphate peak gives the degree of carbonate substitution in the lattice structure of the apatite (Awonusi et al., 2007). Mineral crystallinity, a parameter of mineral maturation, was determined as the inverse the width of the phosphate symmetric-stretch band (ν1 PO_4^{3-} at 960 cm^{-1}) at the half the maximum intensity value ($FWHM^{-1}$) (Yerramshetty and Akkus, 2008). Changes in crystal size and in lattice perfection are reflected in crystallinity measure obtained by using Raman or infrared Spectroscopy since X-ray diffraction methods demand high order of the samples. Specifically for Raman spectroscopy Yerramshetty and co-workers have demonstrated that the *c*-axis length of the crystals is correlated with the mineral crystallinity (Yerramshetty et al., 2006).

3. Results and discussion

The hybrid organic–inorganic coatings applied by sol gel method on surgical grade stainless steel were homogeneous and without evident defects or cracks on the surface, and they also presented good adherence and attachment to the metallic surface (Ballarre et al., 2009b). The barrier effect and corrosion behaviour of these type of silica-based coatings was previously confirmed (Ballarre et al., 2010), as well as their mechanical and adhesive properties (Ballarre et al., 2008, 2009a). The nano-particles of SiO_2 added to reinforce the films, filled the defects and holes present in the silica network, thereby decreasing the porosity and the conductivity of the surface (Montemor et al., 2006). Other possible effect of the addition of amorphous silica into the coating is to promote the biological environment reaction. The use of silica gels as apatite catalyzer and bone promoter was first proposed by Kokubo et al. in 1990 and since then there has been an extended work in this area (Kokubo et al., 1992; Li et al., 1992). The Si presence as silicates at early stages of bone formation seems to be a key path for enhance its kinetics and tissue quality (Matsko et al., 2011; Seaborn and Nielsen, 1994). The combination of glass-ceramic particles with a controlled rate of dissolution of silicon, calcium and phosphorous (Ohtsuki et al., 1992), are thought to play an important role in bone formation around stainless steel implants.

X-ray fluorescence mapping is a useful technique to evaluate Ca, Si and P distribution around the implant in the newly formed bone. Fluorescence maps of the different implanted samples were analyzed. Fig. 2 shows the Ca, P and Si concentration distribution on a *cortical bone* region of 200 by 80 μm of the analyzed femur samples with a 3 μm step. Fig. 2(b) and (c) are optical and histological images of the experimental region. It can be clearly seen the typical bone structure, with Haversian canals (the lowest concentration of Ca, P and Si, were the blood vessels run) and lamellar bone (Dempster, 2005). According to the normalized fluorescence maps, it can be noticed that Ca and P are uniformly distributed in the cortical bone. The intensity minimum in the Ca and P maps

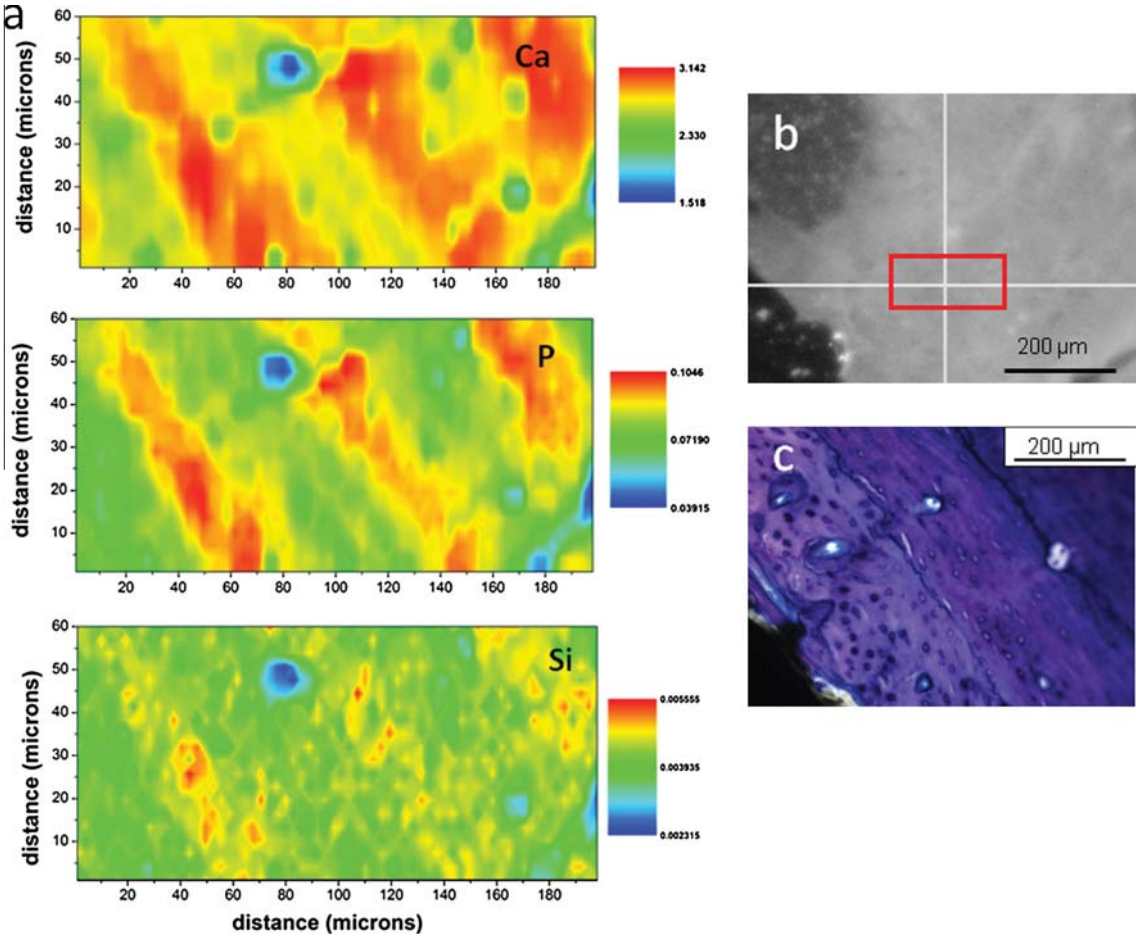

Fig.2. (a) XRF mapping of different elements (Ca, P and Si) of the cortical region from the TMS sample. The x- and y-axis show a micrometer scale, whereas the color bars the intensity of each pixel with the corresponding counts. (b) Optical and (c) histological images of the studied zone.

correspond to the Haversian canals. Silicon remains constant and with a uniform intensity distribution in all zone. It is worth mentioning that using the 7200 eV excitation energy (above the Iron K edge), Iron (Fe) and Chromium (Cr) were not detected in the cortical bone (not shown) which means that there is no diffusion of iron or chromium in the bone tissue.

The concentration of the principal elements related with the HA (Ca and P) in the newly formed bone around the analyzed samples are shown in Figs. 3 and 4. The location of the implant is pointed out from the fluorescence maps with the high content of Fe and Cr. The SS sample seems to create a bone-like interface between the implant and the marrow cavity with a high Ca and P intensity in the outer part of the tissue layer, as can be seen in Fig. 3. The more mineralized bone seems to be created at the beginning of the osseointegration process, and then being separated from the implant. As the authors have discussed in previous related works (Ballarre et al., 2012), early bone formation occurs on SS but it does not progress in time.

Fig. 4 shows the Ca and P intensity maps distribution in the formed tissue between the marrow cavity and the coated implants for the TMS (a) and the TMS-GC (b) samples. The highest intensity (proportional to concentration) of the ions related with apatite in the TMS sample is near the implant, denoting that the growth or mineralization is from the implant to the marrow. The TMS-GC sample shows an almost uniform and high amount of calcium and phosphorous, although the maximum values are in the same range as for the TMS implant sample.

In order to evaluate the bone crystallinity around the implant (marrow and cortical bone) we measured the absorption spectra around the Ca K egde for SS, TMS and TMS-GC samples (Fig. 5). It has been shown that the XANES part of the spectra (20 eV around the absorption edge) can be linked to the bone crystallinity (Laurencin et al., 2010). Indeed the relative intensities of the pre-edge peak and the white line are finger print of atomic ordering around the Ca atoms in the bone.

In the cortical part, the bone is well crystallized and thus can be used as reference in order to estimate the mineralization of a newly formed bone. The SS cortical spectrum presents an intense white line associated to a weak pre edge. These two signatures can be used as fingerprint of a well crystallized part of the bone. In opposite, for SS new bone and TMS new bone, we can observe weaker white line and stronger pre edge peak. This can be related to a much less ordered HA structure. Finally the TMS-GC sample presents the same feature than the SS cortical, meaning that the crystallization is well achieved in this region. This shows, again, that the mineralization of the collagen matrix in the newly formed bone depends on the interface surface and that it has different mineralization profiles.

The EXAFS spectral region is a useful technique used to determine local molecular bonding environments of elements in mineral samples. The EXAFS spectrum contains information on the type and number of atoms in coordination with absorber atoms, their interatomic distances, and the degree of local molecular bonding disorder. As was widely described (Dempster, 2005), bone

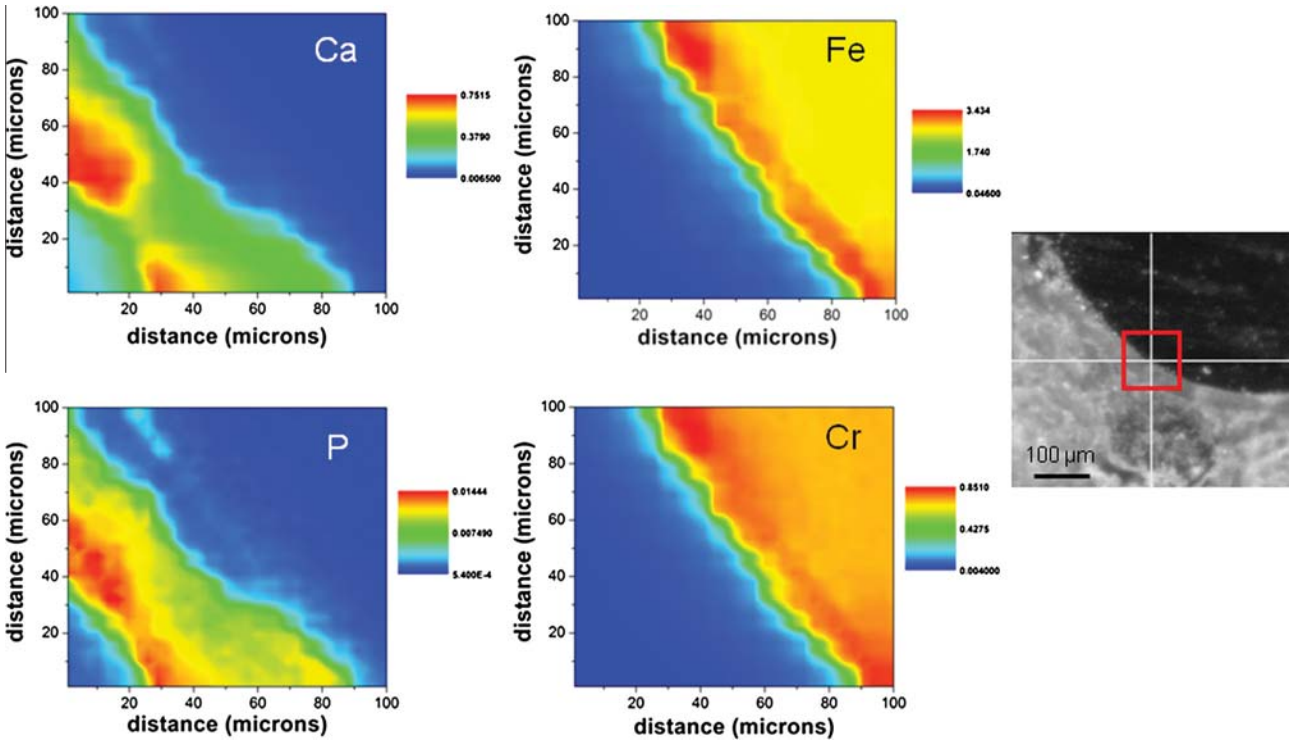

Fig.3. Fluorescence maps for the SS sample implanted in rat femur for 60 days, of different elements (Ca, P, Fe and Cr) in the implant/new bone zone. The *x*- and *y*-axis show a micrometer scale, whereas the color bars the intensity of each pixel with the corresponding counts. Optical image of the mapped zone at the right side of the figure.

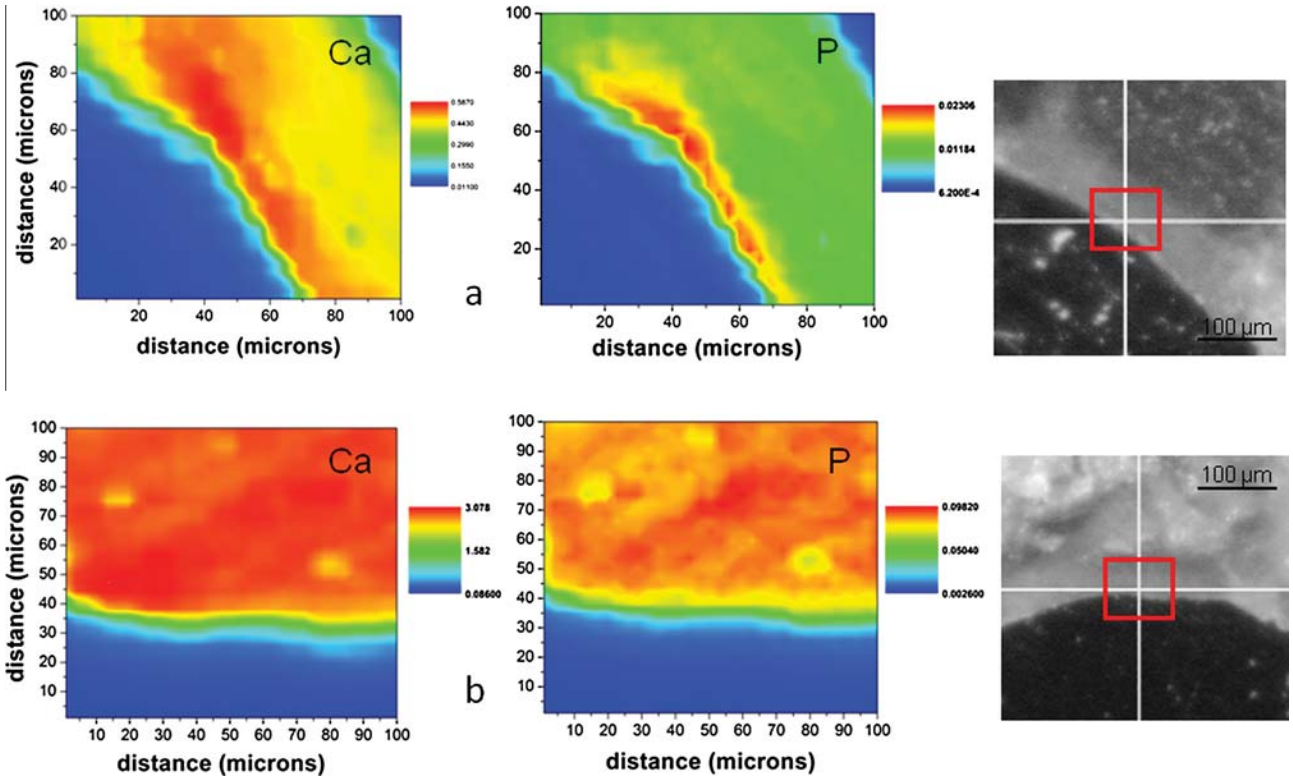

Fig.4. Fluorescence maps of Ca and P elements for the (a) TMS and (b) TMS-GC samples implanted in rat femur for 60 days. The *x*- and *y*-axis show a micrometer scale, whereas the color bars the intensity of each pixel with the corresponding counts. Optical image of the mapped zone at the right side of the figure.

is a composite material with a mineral (some type of carbonate-HA nanocrystals) and an organic (collagen fibrils) part. Also bone is composed by a mixture of amorphous carbonate calcium phosphates with some ion substitution, which will growth with time and to be re-arranging as crystals. In the newly formed bone, a high disorganized structure it is expected to be found. Fig. 6

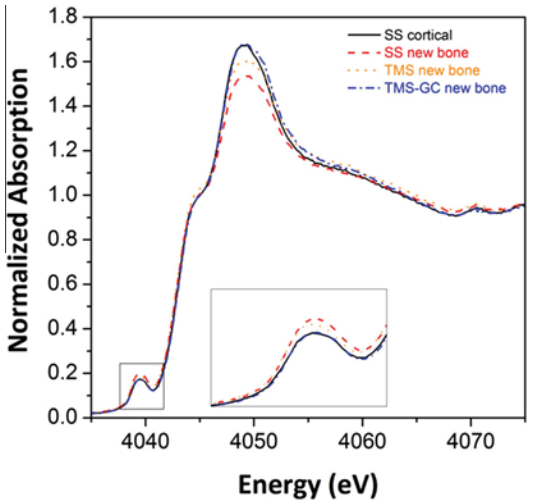

Fig.5. XANES part of the Normalized Absorption spectra for: SS (the cortical zone); and SS, TMS and TMS-GC in the newly-formed bone away from the implant. Inset: detail of the pre edge intensity.

shows the EXAFS spectra and the results of the Fourier-Transform of the three studied samples at the newly-formed tissue zone away from the implant and the cortical bone as reference.

EXAFS oscillations are well defined up to 8 $Å^{-1}$. They are very similar for the three samples but it can be seen much noise on the SS new bone and TMS new bone sample which could be related to a less ordered structure.

The first peak at around 2 Å in Fig. 6 are related with the first two shells of the Ca-O bonding, and the peaks at distance from 3 to 5 Å correspond to shells related to Ca-X unions (Laurencin et al., 2011). In stoichiometric hydroxyapatite (not shown), there are two peaks between 3.5 and 4.5 Å where the first one is more intense than the second, related with a long-range ordering of oxygen, phosphorous and calcium atoms (Harries et al., 1987; Laurencin et al., 2010). In this case, all samples presented no evidence of ordered shells beyond 3.5 Å, caused by the nanocrystalline nature of the apatite crystals in the bone structure, which leads to several sites in the tissue of different environments (Laurencin et al., 2010). In order to analyze clearly the Ca surroundings and the possible substitutions in the lattice, the determination of the relative positions of the neighbouring nuclei should be done. This was not possible in the present work, due to the loss of the long-range ordering after the two first shells, the organic–inorganic nature of the sample and the presence backscattering electrons in the shells. Qualitatively, it can be observed that there is almost no difference between the cortical bone and the layer of tissue formed around the SS and the TMS-GC implanted samples. That means that the disorder of the structure, maturation and the carbonate substitution should be similar (Harries et al., 1987). The TMS sample has a spectrum which is very similar to the one found for bone callus: an unorganized network of woven bone formed at the end of a broken bone that is absorbed as repair is completed (provisional callus), and ultimately replaced by true bone (definitive callus) (Westerman and Scammell, 2012). The raise in intensity of the peak around 4 Å in the SS cortical and TMS-GC samples, could be related with the presence of an increasing degree of crystallinity or growth of the nanocrystals of the bone samples (Peters et al., 2000).

Another interesting tool for analyzing maturity and apatite crystallinity is by microRaman spectroscopy. Raman spectra were obtained and analyzed for the different bone tissue formed around the SS, TMS and TMS-GC coated implants. Fig. 7 shows as an example the spectra of three special regions of interest: metal bulk region, new formed bone and marrow, for the bone tissue analysis. HA (hydroxyapatite, comercial) spectra was included for comparison.

In the newly formed bone and the marrow zone there is embedded material (PMMA) contained in the analyzed matrix. In the marrow, the bands observed at 601, 814, 967, 988, 1454 and 1727 cm^{-1} are associated with PMMA (Matsushita et al., 2000). The most significant peaks of the bone tissue spectra are: the ν1 PO_4 at 960 cm^{-1}, ν2 PO_4 at 430 cm^{-1}, representing the phosphates binding vibrations; CO_3^{2-} at 1071 cm^{-1}, showing beta-carbonates substitutions; and amide I 1643 cm^{-1} and amide III at 1245 cm^{-1}, representing the organic collagen part of the bone tissue. The weak peak at 1643 cm^{-1} is amide I (Gamsjaeger et al., 2010). The amide band I is mostly associated with the C=O stretching vibration due to the presence of collagen (Kazanci et al., 2006), that is present in a lot of organic compounds.

A Raman spectra line scan of 200 microns on the TMS sample is shown in Fig. 8. The progression from the metal, going through the newly formed bone near the implant and finishing in the marrow is plotted to point out the difference in the phosphate peak (960 cm^{-1}) intensity and the peaks related with the embedded material (PMMA, 810 cm^{-1}). As a way to compare the

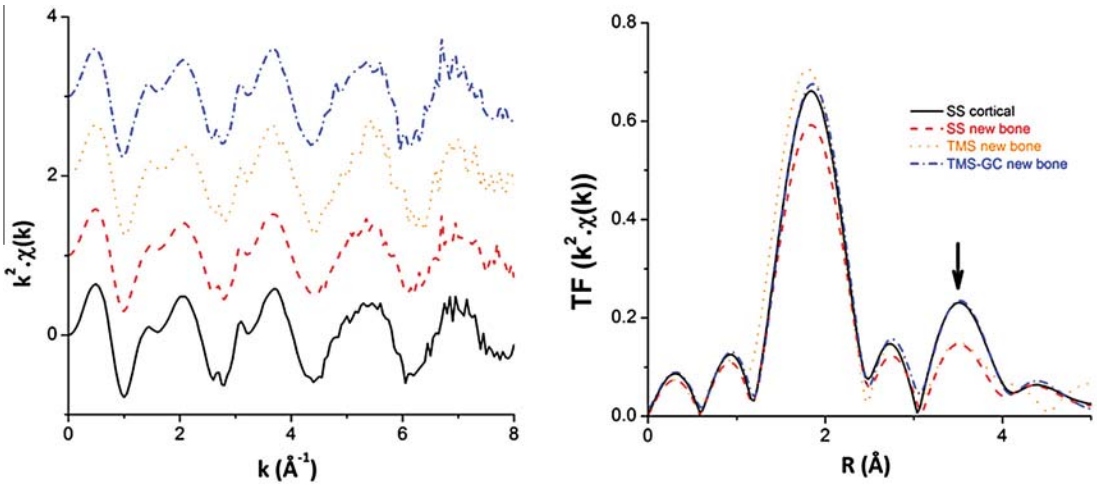

Fig.6. EXAFS spectra and Fourier Transform magnitudes (Ca K-edge, EXAFS spectra) of the bone tissue of three analyzed samples showing the short-range environment of calcium: SS of the cortical zone; and SS, TMS and TMS-GC in the newly-formed bone away from the implant.

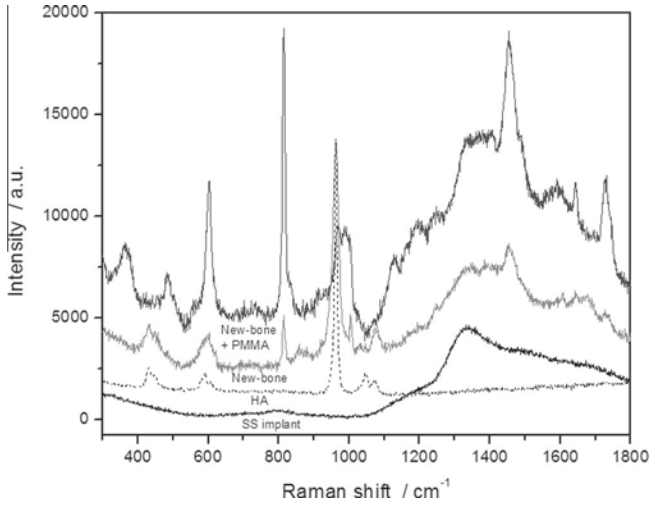

Fig.7. Micro-Raman spectra of three different zones in the TMS sample: The SS implant, the newly-formed bone and the marrow with embedded material PMMA. Commercially pure Hydroxyapatite is shown for comparison.

mineral/collagen relationship and to evaluate the maturity of the bone tissue, several intensities of the Raman spectrum are analyzed. The calculated mean intensities of ν1 PO_4/amide I, ν2 PO_4/amide III and CO_3/ν2 PO_4 bands describe the chemical composition of the bone material. The ν1 PO_4 and amide I bands are not only dependent on the bone composition, but also on the structured orientation (collagen fibrils) (Gamsjaeger et al., 2010). For this study, the mineral to matrix ratio was calculated based on the ν2 PO_4/amide III ratio (both Raman bands are not dependent on spatial orientation hence being related only to composition) (Gamsjaeger et al., 2010). Also it is worth to be notice that the ν2 PO_4^{3-} band is not affected by the presence of PMMA by overlapping of the Raman bands, so there is no need of spectra corrections for the mineral-to-matrix and carbonate-to-phosphate calculations. The choice of matrix band is dependent on the embedding conditions, instrumentation, and its orientational sensitivity (or lack of) toward mineralized collagen fibrils (Morris and Mandair, 2011).

Fig. 9(a) shows the comparison between the cortical and the new formed bone for the three systems studied, regarding the ratio mineral/matrix composition. There are no significant differences between the calculated values for the $_2$ PO_4^{3-}/amide III ratio for the cortex and the new bone at the different zones, but there is a slight change with an increase of the values for the new tissue for the TMS-GC coating. It is possible to be due to the presence of deposited apatite at the surface, acting like a reservoir of Ca and P ions to then nucleate at the collagen fibres and reinforce the structure.

The presence of a carbonate band around 1070 cm^{-1} in the Raman spectrum of the new bone formed (Fig. 7) is significant because it shows phosphate positions in the apatitic lattice are susceptible to ionic substitution (B-type substitution). Raman measurements of carbonate-to-phosphate (CO_3^{2-} ν2 PO_4^{3-}) ratios can provide valuable insights into the chemical composition and maturity or aging of bones. In Fig. 9(b) the carbonate/phosphate substitution for the analyzed samples was plotted. It can be seen that in the case of the SS implant, the new bone formed is identically to the cortical bone, denoting that the tissue was formed at early stages and then remained stable. The coated materials (TMS and TMS-GC) present less carbonate substitution comparing with the cortical bone, what implies that the tissue is still young and continue developing in time. Maturity or carbonate-to-phosphate substitution could be related with mechanical resistance or tissue stiffness.

In previous work (Ballarre et al., 2010), the mechanical properties such hardness and Young modulus of bone tissue were obtained from nanoindentation test. This analysis was done comparing cortical and newly formed bone around stainless steel coated implants with glass-ceramic particles. The mechanical characteristics of bone around non-coated implants was similar to the cortex tissue. With a 10% content of silica nanoparticles in the protective layer and with bioactive particles, the newly formed bone tissue in contact with the cortex (remodellation zone) is softer than the newly formed bone in the marrow region and the indentation modulus and hardness is much lower to the old cortical bone. This implies that the newly bone in contact with the cortex also undergoes remodelling process along with the cortical bone processes.

The strength of bone is not only dependent on the amount of mineralization, but also on the degree of mineral crystallinity and the optimal distribution of different crystal sizes (Donnelly et al., 2010). The most experimentally accessible Raman measure of mineral crystallinity is the width of the primary phosphate band near 960 cm^{-1}. A single Gaussian curve is usually used to fit the phosphate band to obtain the inverse full-width half-maximal ($FWHM^{-1}$) (Morris and Mandair, 2011). The value of the ν1 PO_4^{3-} is affected by the presence of PMMA by overlapping the 960 cm^{-1} band with the 967 and 988 cm^{-1} ones from the C=O component of the acrylic. But as all the samples were equally

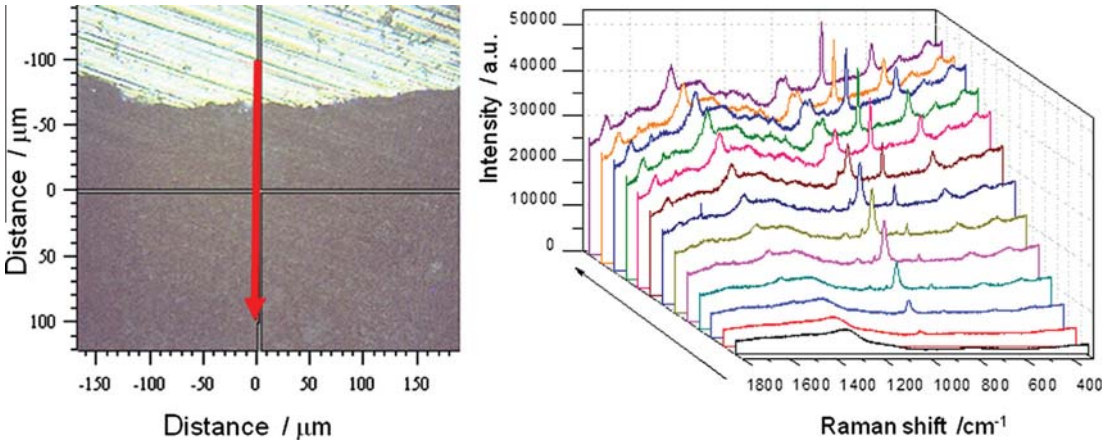

Fig.8. Micro Raman spectroscopy line scan for the TMS simple in the newly-formed tissue zone. (a) Optical image of the analyzed zone. The arrow shows the position and direction of the scan. The total length of the line is 200 µm and the scale is in µm. (b) Sequence of Raman scans during the line.

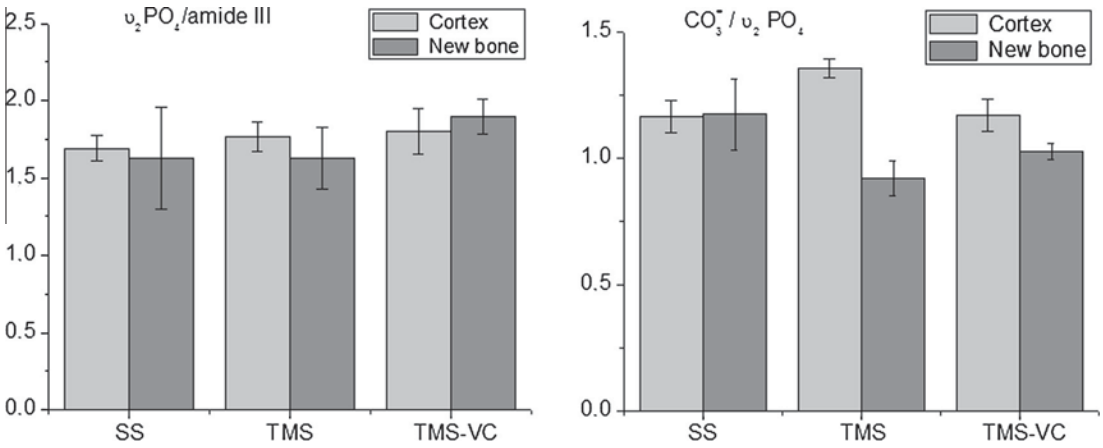

Fig.9. Comparison between the cortical and the new formed bone for the three systems studied (SS, TMS and TMS-GC) regarding: (a) the ratio mineral/matrix composition ($_2$ PO_4^{3-}/amide III ratio), and (b) the degree of carbonate substitution (CO_3/v2 PO_4^{3-}).

Table 2
Crystallinity of the different bone tissue.

Sample	Cortical bone	New formed bone
SS	0.0524 ± 0.0004	0.0506 ± 0.0008
TMS	0.0539 ± 0.0005	0.05 ± 0.0004
TMS-GC	0.0519 ± 0.0003	0.0511 ± 0.0004

The results are expressed as Mean ± SD.

embedded and this ratio is calculated only for make a comparison between the different conditions, the crystallinity parameter obtained with the $FWMH^{-1}$ can be used. The obtained values for crystallinity of the bone tissue around SS, TMS and TMS-GC implants are shown in Table 2. It can be seen that in all the cases, the average crystallinity of the newly formed bone is less than the cortical existing tissue. So in the new bone formed around the coated implants, there is a reduced crystallinity and carbonate substitution. The increase in crystallinity indicates that the crystals are more mature and elongated. Increasing crystal dimensions may affect bone mechanics by inducing residual stresses in their vicinities (Yerramshetty and Akkus, 2008). Small crystals help to give the new bone the necessary strength to support the mechanical solicitations that the system implant-bone is related to in the early stages of fixation. In the case of the SS implant, the degree of carbonate substitution is similar to the cortical bone: non-stoichiometric substitutions are known to modify crystal size, resulting in microstrains within and around the crystal lattice (Handschin and Stern, 1995).

The differences in the spectra and experiments found for the bone tissue around the studied samples show the effect of the interface or initial contact with the treated or not surfaces: when there is no coating, an initial bone tissue is formed: partially mineralized but separated from the implant. The TMS coating clearly induce bone formation and this tissue continue growing, but its characteristics are of a young tissue. The incorporation of silica nanoparticles are thought to act as nucleus for apatite formation, starting with a silica gel formation layer (Li et al., 1993). The presence of silica (usually in silicates or silicic acid form), was discussed earlier by Carlisle and co-workers, claiming the presence of Si in the active areas of early bone formation, showing a decrease of silicon content when the calcium content raises, at the mineralization process starts to end (Carlisle, 1970). This process is clearly improved with the presence of bioactive glass ceramic particles from the SiO_2–P_2O_5–CaO system: the rate of dissolution of the particles is not as high as with glasses, but the phosphates and calcium ions could be slowly release to the media, creating a continuous rich environment for apatitic deposition (Ohtsuki et al., 1992, 1991).

4. Conclusions

The combination of glass-ceramic particles with a controlled rate of dissolution of silicon, calcium and phosphorous, play an important role in bone formation around stainless steel implants. No migration of Fe and Cr was detected for the coated systems in the new formed or in the cortical bone. Mineralized bone tissue is formed around the uncoated implants, but it grows separated from the implant. New bone, attached to the implant and with high concentration of Ca and P close to the implant is found around the samples coated with the hybrid system without glass-ceramic particles. The addition of bioactive particles to the coating enhances the new bone quality, presenting an homogeneous distribution of the Ca and P content in the bone together with a low rate of beta carbonate substitution. These characteristics are analogous to the ones corresponding to a young and mechanically resistant bone.

Acknowledgments

The authors would like to thank A. Cisilino, L. Escalada, Y. Liu and I. Santana, for the grateful help. To the National Research Council of Argentina (CONICET), National Agency for Science and Technology Promotion (ANPCyT – PICT 0917) and National University of Mar del Plata (UNMdP – 15/G331) for financial support. Also would like to acknowledge SOLEIL-France for provision of synchrotron radiation facilities, Cooperation program MinCyT-SOLEIL and Anne-Marie Flank for assistance in application for using beamline.

References

Awonusi, A., Morris, M.D., Tecklenburg, M.M.J., 2007. Carbonate assignment and calibration in the Raman spectrum of apatite. Calcif. Tissue Int. 81, 46–52.
Ballarre, J., López, D.A., Schreiner, W.H., Durán, A., Ceré, S.M., 2007. Protective hybrid sol–gel coatings containing bioactive particles on surgical grade stainless steel: surface characterization. Appl. Surf. Sci. 253, 7260–7264.
Ballarre, J., López, D.A., Cavalieri, A.L., 2008. Nano-indentation of hybrid silica coatings on surgical grade stainless steel. Thin Solid Films 516, 1082–1087.
Ballarre, J., López, D.A., Cavalieri, A.L., 2009a. Frictional and adhesive behavior of organic–inorganic hybrid coatings on surgical grade stainless steel using nano-scratching technique. Wear 266, 1165–1170.
Ballarre, J., Jimenez-Pique, E., Anglada, M., Pellice, S., Cavalieri, A.L., 2009b. Mechanical characterization of nano-reinforced silica based sol–gel hybrid coatings on AISI 316L stainless steel using nanoindentation techniques. Surf. Coat. Technol. 203, 3325–3331.

Ballarre, J., Manjubala, I., Schreiner, W.H., Orellano, J.C., Fratzl, P., Ceré, S., 2010. Improving the osteointegration and bone-implant interface by incorporation of bioactive particles in sol–gel coatings of stainless steel implants. Acta Biomater. 6, 1601–1609.

Ballarre, J., Liu, Y., Mendoza, E., Schell, H., Díaz, F., Orellano, J.C., Fratzl, P., García, C., Ceré, S.M., 2012. Enhancing low cost stainless steel implants: bioactive silica-based sol–gel coatings with wollastonite particles. Int. J. Nano Biomater. 4, 33–53.

Beck Jr., G.R., Ha, S.-W., Camalier, C.E., Yamaguchi, M., Li, Y., Lee, J.-K., Weitzmann, M.N., 2012. Bioactive silica-based nanoparticles stimulate bone-forming osteoblasts, suppress bone-resorbing osteoclasts, and enhance bone mineral density *in vivo*. Nanomed. Nanotechnol. 8, 793–803.

Carlisle, E.M., 1970. Silicon: a possible factor in bone calcification. Science 167, 279–280.

Checmanowski, J.G., Szczygiel, B., 2008. Effect of nanosilica type protective properties of composite ceramic coatings deposited on steel. J Non-Cryst Solids 354, 1786–1795.

Chou, T., Chandrasekaran, C., Cao, G.Z., 2003. Sol–gel derived hybrid coatings for corrosion protection. J. Sol–Gel Sci. Technol. 26, 321–327.

Coathup, M.J., Blunn, G.W., Flynn, N., Williams, C., Thomas, N.P., 2001. A comparison of bone remodelling around hydroxiapatite – coated, porous – coated and grit – blasted hip replacements retrieved at post - mortem. J. Bone Joint Surg. Br. 83-B, 118–123.

Currey, J.D., 2004. Tensile yield in compact bone is determined by strain, post-yield behaviour by mineral content. J. Biomech. 37, 549–556.

Dempster, D.e., 2005. The Bone Quality Book, A Guide to Factors Influencing Bone Strength. Elsevier.

Donnelly, E., Boskey, A.L., Baker, S.P., Van Der Meulen, M.C.H., 2010. Effects of tissue age on bone tissue material composition and nanomechanical properties in the rat cortex. J. Biomed. Mater. Res., Part A 92, 1048–1056.

Flank, A.M., Cauchon, G., Lagarde, P., Bac, S., Janousch, M., Wetter, R., Dubuisson, J.M., Idir, M., Langlois, F., Moreno, T., Vantelon, D., 2006. LUCIA, a microfocus soft XAS beamline. Nucl. Instr. Meth. B 246, 269–274.

Fratzl, P., Gupta, H.S., Paschalis, E.P., Roschger, P., 2004. Structure and mechanical quality of the collagen-mineral nano-composite in bone. J. Mater. Chem. 14, 2115–2123.

Gamsjaeger, S., Masic, A., Roschger, P., Kazanci, M., Dunlop, J.W.C., Klaushofer, K., Paschalis, E.P., Fratzl, P., 2010. Cortical bone composition and orientation as a function of animal and tissue age in mice by Raman spectroscopy. Bone 47, 392–399.

Hanawa, T., 2004. Metal ion release from metal implants. Mater. Sci. Eng., C 24, 745–752.

Handschin, R.G., Stern, W.B., 1995. X-ray diffraction studies on the lattice perfection of human bone apatite (Crista iliaca). Bone 16, 355S–363S.

Harries, J.E., Hasnain, S.S., Shah, J.S., 1987. EXAFS study of structural disorder in carbonate-containing hydroxyapatites. Calcif. Tissue Int. 41, 346–350.

Harries, J.E., Hukins, D.W.L., Hasnain, S.S., 1988. Calcium environment in bone mineral determined by EXAFS spectroscopy. Calcif. Tissue Int. 43, 250–253.

Hastings, G.W., 1980. Biomedical engineering and materials for orthopaedic implants. J. Phys. E: Sci. Instrum. 13, 599–607.

Hing, K.A., Revell, P.A., Smith, N., Buckland, T., 2006. Effect of silicon level on rate, quality and progression of bone healing within silicate – substituted porous hydroxyapatite scaffolds. Biomaterials 27, 5014–5026.

Höland, W., 1997. Biocompatible and bioactive glass – ceramics – state of the art and new directions. J. Non-Cryst. Solids 219, 192–197.

Kazanci, M., Roschger, P., Paschalis, E.P., Klaushofer, K., Fratzl, P., 2006. Bone osteonal tissues by Raman spectral mapping: orientation-composition. J. Struct. Biol. 156, 489–496.

Kokubo, T., Kushitani, H., Ohtsuki, C., Sakka, S., 1992. Chemical reaction of bioactive glass and glass – ceramics with a simulated body fluid. J. Mater. Sci.: Mater. Med. 3, 79–83.

Laurencin, D., Wong, A., Chrzanowski, W., Knowles, J.C., Qiu, D., Pickup, D.M., Newport, R.J., Gan, Z., Duer, M.J., Smith, M.E., 2010. Probing the calcium and sodium local environment in bones and teeth using multinuclear solid state NMR and X-ray absorption spectroscopy. Phys. Chem. Chem. Phys. 12, 1081–1091.

Laurencin, D., Almora-Barrios, N., de Leeuw, N.H., Gervais, C., Bonhomme, C., Mauri, F., Chrzanowski, W., Knowles, J.C., Newport, R.J., Wong, A., Gan, Z., Smith, M.E., 2011. Magnesium incorporation into hydroxyapatite. Biomaterials 32, 1826–1837.

Li, P., Ohtsuki, C., Kokubo, T., Nakanishi, K., Soga, N., Nakamura, T., Yamamuro, T., 1992. Apatite formation induced by silica gel in simulated body fluid. J. Am. Ceram. Soc. 75, 2094–2097.

Li, P., Ohtsuki, C., Kokubo, T., Nakanishi, K., Soga, N., Nakamura, T., Yamamuro, T., 1993. Process of formation of bone-like apatite layer on silica gel. J. Mater. Sci.: Mater. Med. 4, 127–131.

Matsko, N.B., Žnidaršič, N., Letofsky-Papst, I., Dittrich, M., Grogger, W., Štrus, J., Hofer, F., 2011. Silicon: the key element in early stages of biocalcification. J. Struct. Biol. 174, 180–186.

Matsushita, A., Ren, Y., Matsukawa, K., Inoue, H., Minami, Y., Noda, I., Ozaki, Y., 2000. Two-dimensional Fourier-transform Raman and near-infrared correlation spectroscopy studies of poly(methyl methacrylate) blends. 1. Immiscible blends of poly(methyl methacrylate) and atactic polystyrene. Vib. Spectrosc. 24, 171–180.

Montemor, M.F., Cabral, A.M., Zheludkevich, M.L., Ferreira, M.G.S., 2006. The corrosion resistance of hot dip galvanized steel pretreated with Bis-functional silanes modified with microsilica. Surf. Coat. Technol. 200, 2875–2885.

Morris, M.D., Mandair, G.S., 2011. Raman assessment of bone quality. Clin. Orthop. Relat. R 469, 2160–2169.

Ohtsuki, C., Kushitani, H., Kokubo, T., Kotani, S., Yamamuro, T., 1991. Apatite formation on the surface of ceravital – type glass – ceramic in the body. J. Biomed. Mater. Res. 25, 1363–1370.

Ohtsuki, C., Kokubo, T., Yamamuro, T., 1992. Mechanism of apatite formation on $CaO–SiO_2–P_2O_5$ glasses in a simulated body fluid. J. Non-Cryst. Solids 143, 84–92.

Peitl, O., Zanotto, E.D., Hench, L.L., 2001. High bioactive $P_2O_5–Na_2O–CaO–SiO_2$ glass – ceramic. J. Non-Cryst. Solids 292, 115–126.

Peters, F., Schwarz, K., Epple, M., 2000. The structure of bone studied with synchrotron X-ray diffraction, X-ray absorption spectroscopy and thermal analysis. Thermochim. Acta 361, 131–138.

Seaborn, C.D., Nielsen, F.H., 1994. Effects of germanium and silicon on bone mineralization. Biol. Trace Elem. Res. 42, 151–164.

Westerman, R.W., Scammell, B.E., 2012. Principles of bone and joint injuries and their healing. Surgery (Oxford) 30, 54–60.

Yerramshetty, J.S., Akkus, O., 2008. The associations between mineral crystallinity and the mechanical properties of human cortical bone. Bone 42, 476–482.

Yerramshetty, J.S., Lind, C., Akkus, O., 2006. The compositional and physicochemical homogeneity of male femoral cortex increases after the sixth decade. Bone 39, 1236–1243.